Journal of Materials Science: Materials in Medicine (2018) 29:126
https://doi.org/10.1007/s10856-018-6137-2

BIOMATERIALS SYNTHESIS AND CHARACTERIZATION

Original Research

# The preparation of heparin-like hyperbranched polyimides and their antithrombogenic, antibacterial applications

Qing Li[1,2] · Jing Li[2] · Guangfu Liao[3] · Zushun Xu[2]

Received: 25 November 2017 / Accepted: 20 July 2018 / Published online: 28 July 2018


## Abstract

1,3,5-Tris(4-aminophenoxy) benzene (TAPOB) and 2,2-bis [4-(3,4-dicarboxyphenoxy) phenyl] propane dianhydride (BPADA) were used to synthesize an amino-terminated hyperbranched polyimide (AM-HBPI). Then, the 2-methacryloyloxyethyl phosphorylcholine-modified hyperbranched polyimide (HBPI-MPC) was obtained through the graft modification of MPC onto AM-HBPI by Michael addition. The infrared spectroscopy and X-ray photoelectron spectroscopy spectra showed MPC molecules were successfully grafted onto the HBPI molecules. The HBPI-MPC films exhibited slightly decreased thermal stabilities with 5% weight loss temperature in the range of of 418–483 °C in nitrogen, compared with the pure HBPI film. With the increase of MPC grafting amount, the static water contact angles decreased from average 84.0° of the pure HBPI film to average 45.0° of the HBPI-MPC film with 20% MPC. Meanwhile, the increased surface roughness of the HBPI-MPC films increased the contact areas with the platelets, enhancing their anticoagulant efficiency. The number of platelet adhesion declined and the shape of platelet changed from flat to round. The recalcification times grew from average 300 s of pure HBPI to average 551 s of the HBPI-MPC film with 20% MPC, indicating improved anticoagulant properties and biocompatibility. Bacterial adhesion test also demonstrated the number of bacterial adhesion was significantly reduced and antibacterial properties were improved. Thus, the HBPI-MPC films have great application prospects as biomedical anticoagulant materials.

## Graphical Abstract

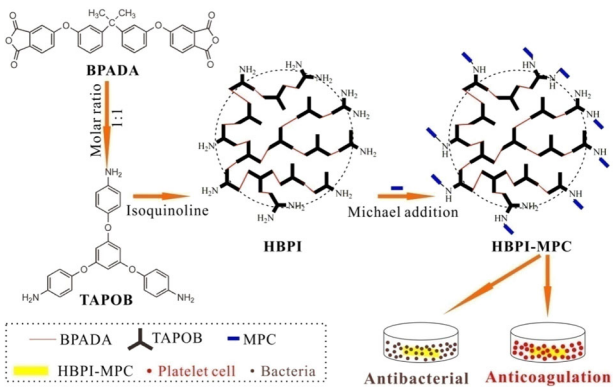


These authors contributed equally: Qing Li, Jing Li.

✉ Zushun Xu
zushunxu@hubu.edu.cn

[1] Guangxi Key Laboratory of Chemistry and Engineering of Forest Products, School of Chemistry and Chemical Engineering, Guangxi University for Nationalities, 530008 Nanning, Guangxi, China

[2] Hubei Collaborative Innovation Center for Advanced Organic Chemical Materials; Ministry of Education Key Laboratory for the Green Preparation and Application of Functional Materials, Hubei University, 430062 Wuhan, Hubei, China

[3] School of Materials Science and Engineering, PCFM Lab, Sun Yat-Sen University, 510275 Guangzhou, China

## 1 Introduction

In recent years, anticoagulant materials have received widespread attentions and are widely used in biomedical fields, such as hemodialysis systems, extracorporeal circulation systems, cardiac valve repair, pacemakers, blood vessel prosthesis and intravascular stent [1–3]. The related researches have also made great progress. Many polymer biomaterials have been developed, such as polymethylmethacrylate (PMMA), polyethylene (PE), polypropylene (PP), polysulfone (PSF), polyethersulfone (PES), polyimide (PI) and so on [4–8]. Because of good mechanical properties and a certain degree of biocompatibility, they can be used as anticoagulant materials. However, the main factor in determining whether the polymer materials can be used as biomedical materials is whether their anticoagulation is good enough. Although PMMA, PES, PI, etc. are generally used as matrix materials, they still need to be modified due to poor biocompatibility [9]. In order to improve their biocompatibility, surface modification is a fairly ideal method. The material and technology used for surface modification have been developed rapidly, including grafting negatively charged or biological macromolecules such as bovine serum albumin and heparin, grafting zwitterionic polymers, designed as a microphase separation structure, inoculated with endothelial cells and so on. In practical applications, these surface modifications endow polymer materials with excellent performance and specific biological properties [10]. However, the most commonly used biological materials, such as heparin materials, polyphosphorylcholine and polyethylene glycol can not fully meet the clinical application. The reasons are shown as follows. First, the anticoagulant activities of these materials are insufficient after long-term implantation of human. Second, their antibacterial properties are poor and bacterial infection is easy to be caused, resulting in a variety of complications. Therefore, it is of great significance to improve the anticoagulant activity, antibacterial properties and blood compatibility of this kind of anticoagulant materials [11].

The researches of the early bionic surface coating focused on the synthesis of natural lipid dipalmitoylphosphatidylcholine (DPPC) with alkynyl functional groups on its alkyl chains. Biocompatible diacetylphosphatidylcholine (DAPC) coating can be synthesized by ultraviolet (UV) or γ-ray irradiation [12, 13]. Meanwhile, it was reported that the active small molecule derivatives of phosphatidyl choline (PC) were chemically coupled directly to the appropriate functionalized surface. Another approach dominated by Japan was the development of phospholipid-based monomers and polymer derivatives [14].

As novel biological materials, methacrylate and 2-methacryloyloxyethyl phosphorylcholine (MPC, the structural formula shown in Scheme 1) were developed by Nakabayashi group [12]. They demonstrated these

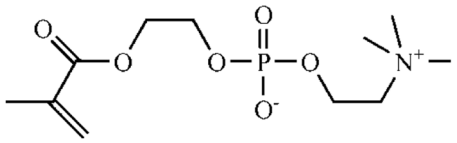

**Scheme 1** The structural formula of MPC

containing lipid-based substances had potential applications in biomedical fields. Researchers believed that the obtained surface structures were closer to the structures of natural cell membrane lipid after the MPC with alkyl methacrylate long chains was copolymerized to the surfaces of some substances. These MPC molecules were amphiphilic, including highly polar zwitterionic PC groups and hydrophobic alkyl chains. The hydrophobic materials will have extremely stable biocompatibility when these materials are dissolved in a suitable solvent and the obtained solutions are coated on hydrophobic materials by physical means [15]. Researchers have done a lot of structural changes to these simple copolymers, incuding the introduction of special groups that chemically couples to the surface of the materials, the introduction of urethane side chains to enhance the interaction between the polyurethane and the coating, adding crosslinking agent to improve the physical properties of the film, the introduction of cationic copolymers to be grafted with special functional groups such as heparin [16, 17]. In addition, there are more complex methods including the synthesis of poly(n-butyl methacrylate)-graft-poly(2-methacryloyloxyethyl phosphorylcholine) (PBMA-g-PMPC) by copolymerization of macromonomer MPC and n-butyl methacrylate (BMA) [18].

Polyimides (PIs) are one of the most important high performance and advanced polymers, which possess excellent mechanical properties, thermal stability, chemical resistance and low dielectric constant. Hence, they are widely applied in the fields of aviation, aerospace, microelectronics, liquid crystal, separation film and laser [19–22]. Moreover, PIs have good biocompatibility, non-hemolytic, non-toxic in vitro cells and even withstand thousands of sterilization [23, 24]. Therefore, they also have a wide range of applications in the biomedical fields.

In view of the unique three-dimensional tree structure, a large number of terminal functional groups, low solution viscosity and vast internal gaps of hyperbranched polymers, they are greatly favored in the field of biomedical materials [25–31]. In this article, we have prepared a amino-terminated hyperbranched polyimide (HBPI) based on a triamine 1,3,5-tris(4-aminophenoxy) benzene (TAPOB) and a commercial dianhydride 2,2-bis[4-(3,4-dicarboxyphenoxy)phenyl] propane dianhydride (BPADA). Then, the MPC-modified HBPI (HBPI-MPC) were obtained by Michael addition reaction. Moreover, we tested the thermal properties, surface properties, anticoagulant properties,

hemocompatibility and antibacterial properties of HBPI-MPC films. Results showed they had the possibility of long-term use as biomedical instrument materials.

## 2 Experimental section

### 2.1 Materials

1,3,5-tris(4-aminophenoxy) benzene (TAPOB) was synthesized according to Chen's work [32]. 2,2-bis[4-(3,4-dicarboxyphenoxy)phenyl]propane dianhydride (BPADA) were purchased from Shanghai Research Institute of Synthetic Resins (Shanghai, China). 2-methacryloyloxyethyl phosphorylcholine (MPC, 96%) was obtained from J&K Scientific Ltd. N-methyl-2-pyrrolidone (NMP, HPLC grade) and isoquinoline (97%) were purchased from Aladdin Industrial Corporation (Shanghai, China), which were used as received. Ethanol (AR, 99.7%), $KH_2PO_4$ (AR, 99.5%), $Na_2HPO_4$ (AR, 99.0%), $Na_2HPO_4{\cdot}12H_2O$ (AR, 99.0%), NaCl (AR, 99.5%), KCl (AR, 99.5%), $CaCl_2$ (AR, 96.0%) and glutaraldehyde (BR, 25% aqueous solution) were purchased from Sinopharm Chemical Reagent (Shanghai, China). Fresh human blood (3.8% sodium citrate as anticoagulant) and Staphylococcus aureus (physiological saline as solvent) were provided by Wuhan Union Hospital.

### 2.2 Preparation of amino-terminated hyperbranched polyimide (AM-HBPI)

The hyperbranched polyimide was synthesized from a triamine TAPOB and a commercial aromatic dianhydride BPADA. Thereinto, TAPOB was synthesized by referring to Chen's work [32]. The one-step polycondensation method for preparation of AM-HBPI was adopted, as the specific procedure shown below. 1.0 mmol TAPOB was first dissolved in 10 mL NMP under $N_2$ flow in an ice bath, then 1.0 mmol BPADA in 10 mL NMP was added dropwise through a syringe. After stirring for 1 h, isoquinoline (ca. 5 drops) was added, and the solution was further stirred for 5 h at 120 °C, then the mixture was heated at 180 °C for 24 h. Brown fibrous precipitates were obtained when the resultant polymer solutions were poured into an excess of ethanol. The polymers were separated by filtration and washed with ethanol for several times then dried under vacuum oven at 100 °C for 24 h.

### 2.3 Preparation of 2-methacryloyloxyethyl phosphorylcholine-modified HBPI (HBPI-MPC) films

AM-HBPI was grafted by the following procedures as shown in Scheme 2. MPC (prescribed amount, i.e., 0, 5, 10, 15 and 20 wt.% of HBPI) was added into HBPI solution in NMP, and the mixture was stirred for 24 h to form a homogeneous mixture. Subsequently, the mixture was poured into a level glass plate with silicone mold and dried at 80 °C for 12 h until an equilibrium weight was achieved, and heated at 100 °C for 1 h, 150 °C for 1 h, 200 °C for 1 h, successively. The prepared films were cooled down naturally and peeled off. The films were then shaken in deionized water at room temperature for 5 h to remove ungrafted MPC. This washing step was repeated three times. Finally, the resulting HBPI-MPC films were dried to constant weight in vacuum at room temperature. They were respectively named as HBPI, HBPI-5MPC, HBPI-10MPC, HBPI-15MPC, HBPI-20MPC.

### 2.4 Preparation of phosphate buffered solution (PBS, pH = 7.4, 0.01 mol/L)

0.27 g $KH_2PO_4$, 1.42 g $Na_2HPO_4$, 3.58 g $Na_2HPO_4{\cdot}12H_2O$, 8.00 g NaCl, 0.20 g KCl were dissolved in deionized water. And transfer the solution to a 1 L volumetric flask. Shake to spare after settling to permit.

### 2.5 In vitro platelet adhesion test

Fresh human blood (3.8% sodium citrate as anticoagulant) was centrifuged at 2000 r/min for 15 min to collect upper platelet-rich plasma (PRP). The samples ($0.5 \times 0.5\ cm^2$) were soaked in PBS for 24 h to achieve swelling equilibrium. The samples were kept in PRP solution for 1.5 h at 37 °C. The PRP was removed with an aspirator, and each film was rinsed three times with 3 mL of PBS. Then, 3 mL of 2.5 vol% glutaraldehyde in PBS was poured into each well, and the materials were maintained at room temperature for 30 min to fix the platelet on the film. The film was washed with PBS again and then subsequently dehydrated by systemic immersion in a series of ethanol water solutions (50, 60, 70, 80, 90, 95, and 100% (v/v)) for 30 min each and allowed to evaporate at room temperature. Repeat the platelet adhesion test twice again.The surfaces of the obtained fifteen films with platelets were observed with a scanning electronic microscope (SEM; JEOL, Japan) following gold-sputtering on the film surface. For SEM, three areas on each sample were observed, and the presented images are representative. Quantification of adhered platelets was performed by calculating the total platelet surface coverage from the obtained nine images of one sample using SEM images.

### 2.6 Plasma recalcification time (PRT) test

The samples ($10 \times 10\ mm^2$) were immersed in physiological saline for 24 h to reach swelling equilibrium. The samples

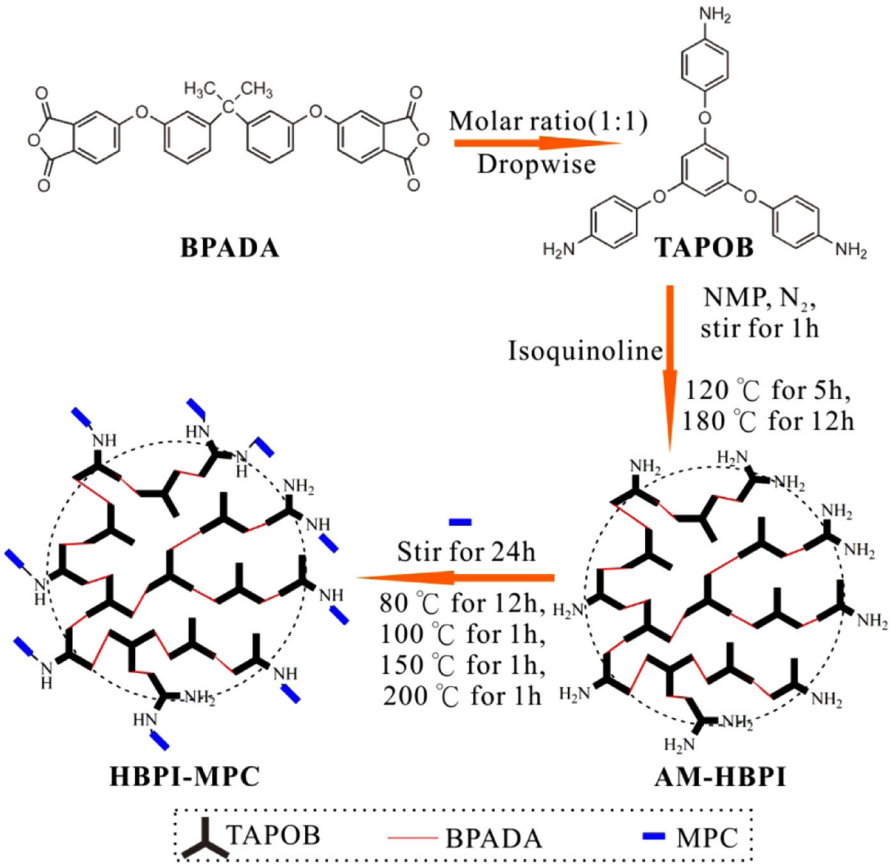


**Scheme 2** The synthesis process diagram of HBPI-MPC films

were added to a polypropylene tube containing 1.5 mL of plasma in 37 °C constant temperature water bath. Then 0.2 mL of $CaCl_2$ (0.1025 mol/L) was added. The tube was shaking at 37 °C bath, and the process began to be monitored.The stopwatch started timing, and stoped when the silky fibrin appeared [33]. Repeat the PRT test twice again.

## 2.7 Antibacterial adhesion test

Staphylococcus aureus were used to evaluate the antibacterial activity of samples. Typically, bacteria were cultured with a Luria-Bertani (LB) culture medium. According to the standard procedure, sterile LB broth and LB agar plates were prepared. All disks and materials were sterilized in an autoclave before experiments. The samples (0.5 × 0.5 $cm^2$) were placed into five 96-well plate, and 200 μL of Mcfarland Turbidity 0.5 of Staphylococcus aureus (physiological saline as solvent) was added into each well with one sample. They are in 37 °C constant temperature water bath for 1 h. Then, 3 mL of 2.5 vol% glutaraldehyde in PBS was poured into each well, and the materials were maintained at room temperature for 30 min to fix the Staphylococcus aureus on the films. The films were washed with PBS again and then subsequently dehydrated by systemic immersion in a series of ethanol water solutions (50, 60, 70, 80, 90, 95, and 100% (v/v)) for 30 min each and allowed to evaporate at room temperature. The surfaces of the films with Staphylococcus aureus were observed with a scanning electronic microscope (SEM; JEOL, Japan) following gold-sputtering on the film surface. Repeat the antibacterial adhesion test twice again. For SEM, three areas on each sample were observed, and the presented images are representative. Quantification of adhered staphylococcus aureus was performed by calculating the total staphylococcus aureus surface coverage from the obtained nine images of one sample using SEM images.

## 2.8 Characterization

Fourier transform infrared (FTIR) spectra were recorded on a Nicolet iS50 spectrometer (Thermo Fisher Scientific, USA); thereinto, fourier-transformed infrared spectra of the films in a single-beam modus were measured in the attenuated total reflection modus. The hydrogen-1 nuclear magnetic resonance ($^1$H NMR) analysis was recorded by a Varian INOVA-400 spectrometer (Salt Lake City, Utah, USA), DMSO-$d_6$ as a solvent, and tetramethylsilane as an

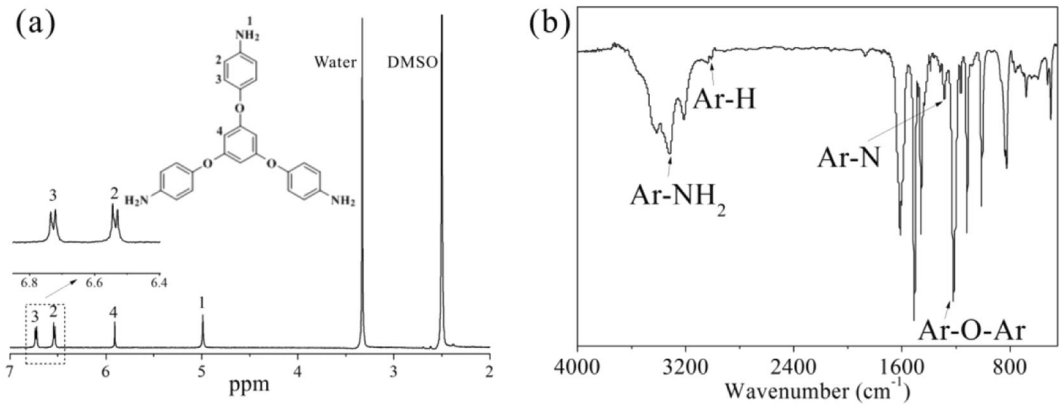


**Fig. 1** The **a** $^{1}$H NMR and **b** FTIR spectra of TAPOB

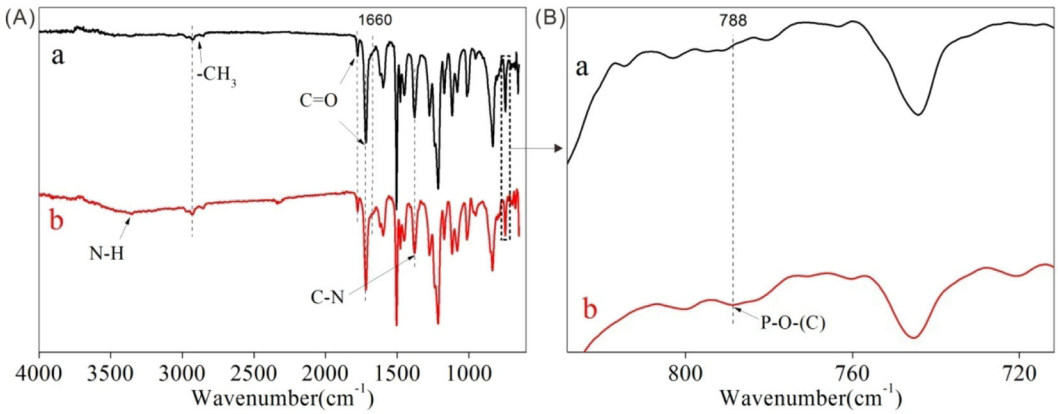


**Fig. 2** **a** The FTIR spectra of HBPI film and HBPI-15MPC film; **b** the enlarged view in the dashed box in **a**

internal standard. Thermogravimetric analysis (TGA) were carried out with a Perkin-Elmer TGA-7 thermal gravimetric analyzer at a heating rate of 20 °C/min from 30 to 800 °C under nitrogen flow. UV-vis spectra were measured with a Shimadzu UV-3600 spectrometer in the transmittance mode. X-ray photoelectron spectroscopy (XPS) measurement was carried out on an AXIS Ultra X-ray photoelectron spectrometer (Thermo Fisher Scientific Escalab 250Xi). Water surface contact angle (WSCA) test was conducted on JC2000 D instrument (Shanghai, China). Atomic force microscopy (AFM) was carried out by using an SOLVER NANO SPM from NT-MDT. The topography of the surfaces of these films were studied by AFM, using a Dimension 3100 AFM from the Veeco-Digital Instruments (Santa Barbara, CA). In each case, an area of $40 \times 40\ \mu m^2$ was scanned using the tapping mode. The drive frequency of the equipment, with a voltage between 3.0 and 4.0 V, was 330 ± 50 kHz. The drive amplitude was about 300 mV, and the scan rate was 0.5–1.0 Hz. The arithmetic mean of the surface roughness (Ra) reported was calculated from the roughness profile determined by AFM.

## 3 Results

### 3.1 Synthesis of monomer TAPOB

The characterization of the triamine monomer TAPOB was shown in Fig. 1. The $^{1}$H NMR spectrum of TAPOB is shown in Fig. 1a. The specific attributions include $^{1}$H NMR (600 MHz, DMSO-$d_6$, δ, ppm), 6.72 (d, 6H, H3), 6.53 (d, 6H, H2), 5.91 (s, 3H, H4), 4.99 (s, 6H, H1). Infrared spectroscopy was also used to characterize the structure of the monomer TAPOB, as shown in Fig. 1b. In the FTIR spectrum of triamine monomer TAPOB, four characteristic absorption peaks appeared respectively at 3320 $cm^{-1}$ (Ar-$NH_2$), 3015 $cm^{-1}$ (Ar-H), 1290 $cm^{-1}$ (Ar-N) and 1213 $cm^{-1}$ (Ar-O-Ar).

### 3.2 Structures of HBPI and HBPI-MPC films

In addition to the sizes of the peaks, the FTIR and XPS spectra of HBPI-MPC films are basically the same. Thus, we chose HBPI-15MPC as an example and measured its FTIR and XPS spectra. Figure 2 shows FTIR absorption of

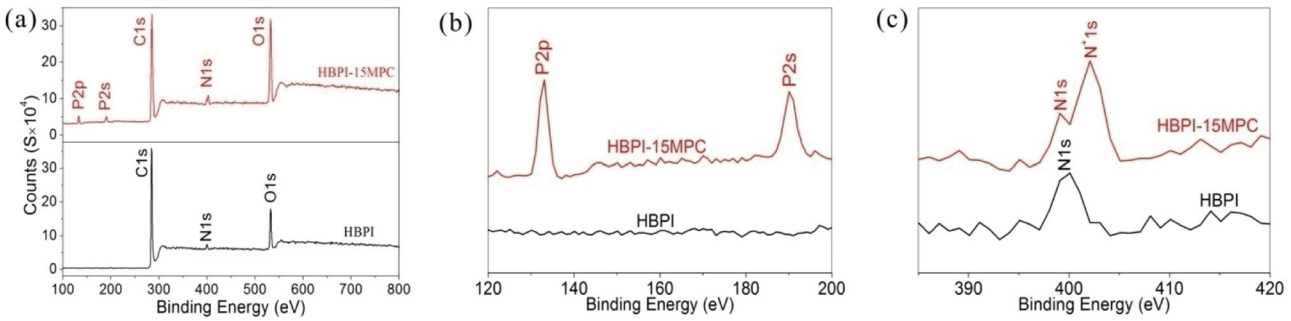


**Fig. 3** **a** The overview XPS spectra of HBPI film and HBPI-15MPC film; **b** XPS P2p and **c** N1s narrow-scan spectra of HBPI film and HBPI-15MPC film

**Table 1** The thermal property of HBPI-MPC films

| Samples | $T_{d,5}$(°C) | $T_{d,10}$(°C) | $R_w$(wt.%) |
|---|---|---|---|
| HBPI | 496.7 | 522.7 | 59.7 |
| HBPI-5MPC | 483.0 | 516.7 | 65.9 |
| HBPI-10MPC | 450.0 | 495.3 | 67.1 |
| HBPI-15MPC | 435.3 | 479.0 | 66.6 |
| HBPI-20MPC | 418.7 | 462.3 | 64.0 |

$T_{d,5}$: the temperature at 5% weight loss

$T_{d,10}$: the temperature at 10% weight loss

$R_w$: residue weight at 800 °C

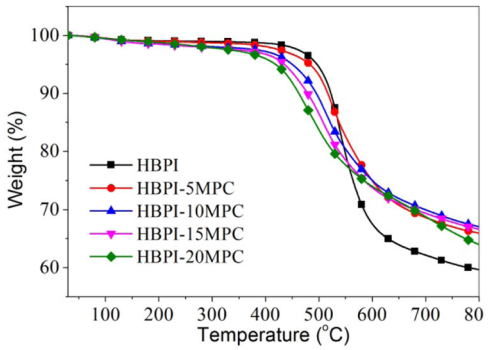


**Fig. 4** The TGA curves of HBPI-MPC films

amino-terminated HBPI based on BPADA and TAPOB. There was no absorption band at 1660 $cm^{-1}$. Compared to Fig. 2a, panel a, two new peaks appeared at 3354 and 788 $cm^{-1}$ in Fig. 2a, panel b, which were sequentially attributed to N-H, P-O-(C).

XPS can be also used to characterize the surface composition and chemical structure of HBPI and HBPI-15MPC films. Figure 3 presents the overview XPS spectra, as well as XPS P2p, P2s and N1s narrow-scan spectra of HBPI and HBPI-15MPC film. As shown in Fig. 3a, the XPS spectrum of HBPI-MPC shows the additional presence of P2p (around 133 eV) and P2s (around 190 eV) except C1s (around 284 eV), N1s (around 400 eV), and O1s (around 533 eV), compared with that of HBPI. Specifically, in Fig. 3b, the narrow-scan XPS spectrum of HBPI-15MPC film exhibits two main peaks, which are ascribed to P2p and P2s. However, there is no peaks in the narrow-scan XPS spectrum of HBPI. In addition, as Fig. 3c shown, the N1s peak of HBPI film splits into two peaks of HBPI-15MPC film, which are assigned to N1s (399 eV) and the $N^+$ characteristic peak in $N^+(CH_3)_3$ (402 eV), respectively.

## 3.3 Thermal properties

The thermal properties of HBPI-MPC films were examined by means of thermogravimetric analysis (TGA). Table 1 summarizes the thermal properties of HBPI-MPC films. The TGA curves of HBPI-MPC films are shown in Fig. 4. The addition of MPC slightly decreased thermal stability of neat HBPI whose $T_{d,5}$ and $T_{d,10}$ are 496.7 °C, 522.7 °C, respectively. The $T_{d,5}$s of HBPI-5MPC, HBPI-10MPC, HBPI-15MPC, HBPI-20MPC were 483.0 °C, 450.0 °C, 435.3 °C, 418.7 °C, respectively. The $T_{d,10}$s of HBPI-5MPC, HBPI-10MPC, HBPI-15MPC, HBPI-20MPC were 516.7 °C, 495.3 °C, 479.0 °C, 462.3 °C, respectively. Moreover, the initial decomposition temperature also slightly decreased with the increase of MPC grafting amount.

## 3.4 Surface properties

The surface properties of HBPI-MPC films were investigated by means of water surface contact angle (WSCA) and atomic force microscope (AFM). As shown in Fig. 5a, the neat HBPI film exhibited an average WSCA of 84.0°. With the increase of MPC grafting amount, the HBPI-MPC films exhibited decreased WSCA values (Fig. 5b) from 84.0° to the minimum 45.0°.

Topographies of HBPI, HBPI-5MPC, HBPI-10MPC, HBPI-15MPC, HBPI-20MPC films were observed by AFM (Fig. 6). In addition, roughness parameter (Ra) values of the films, which are applied to describe the surface roughness, are intuitively displayed in Fig. 7. The image of the

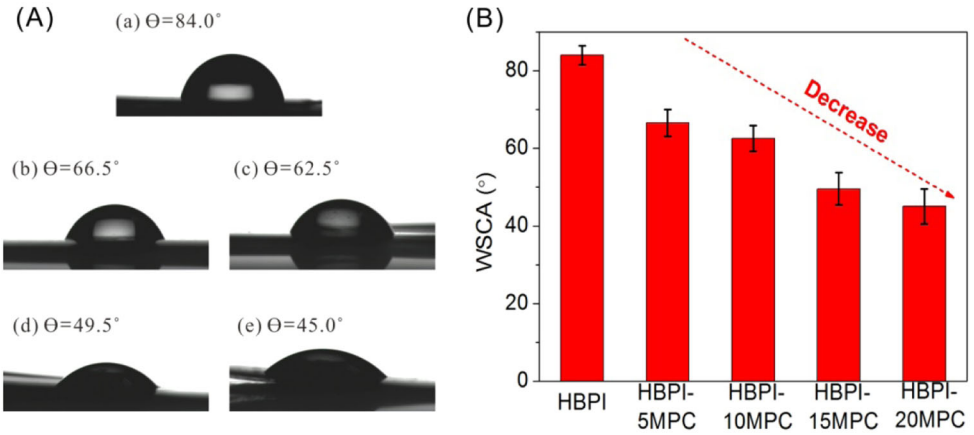


**Fig. 5** Pictures **a** and histogram **b** for the water surface contact angles of HBPI-MPC films: HBPI **a**, HBPI-5MPC **b**, HBPI-10MPC **c**, HBPI-15MPC **d**, HBPI-20MPC **e**

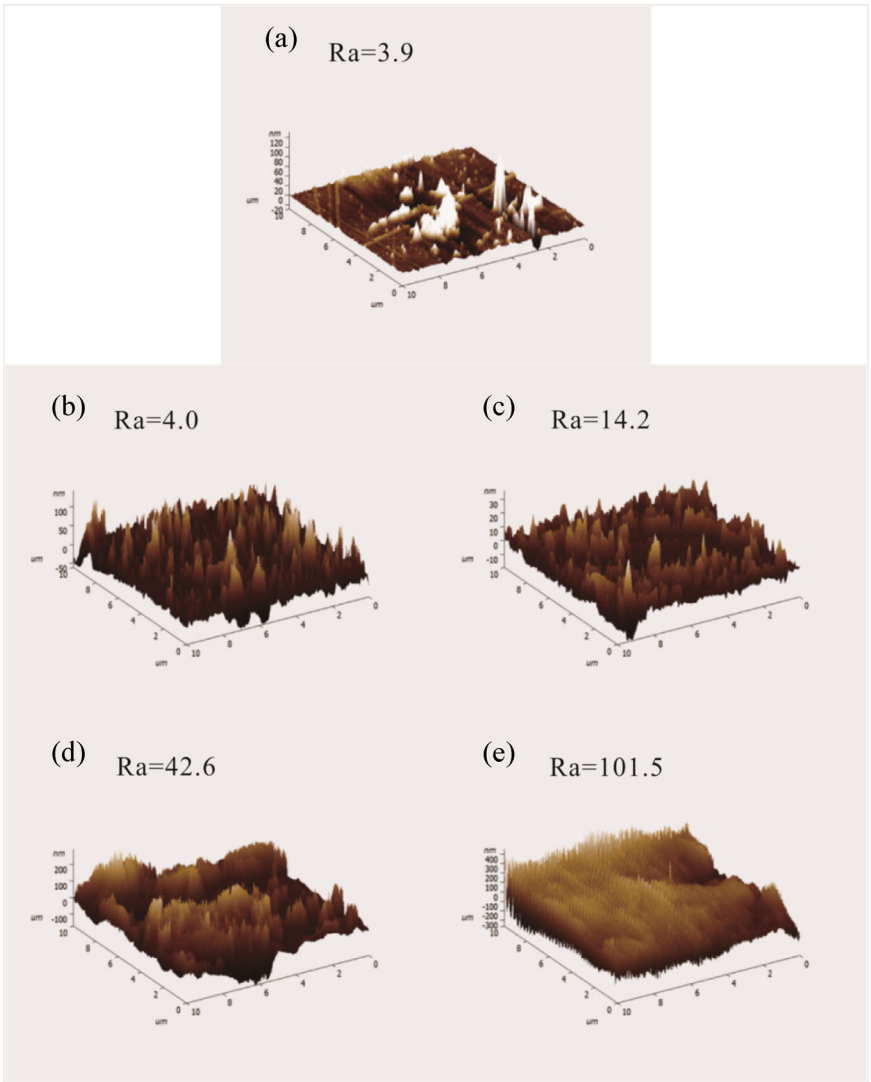


**Fig. 6** The AFM pictures of HBPI-MPC films: **a** HBPI, **b** HBPI-5MPC, **c** HBPI-10MPC, **d** HBPI-15MPC, **e** HBPI-20MPC

relatively smooth PI surface was observed (Fig. 6a). With the increase of MPC grafting amount, the HBPI-MPC films exhibited increased surface roughness, which was consistent with the Ra values for the surface (Fig. 7). The Ra value for HBPI-20MPC film was largest (101.5 nm) among the tested films, indicating the largest surface roughness.

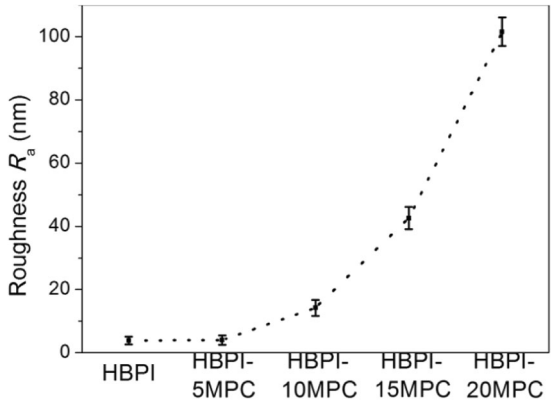


**Fig. 7** Values of roughness parameter (Ra) for the surfaces obtained from AFM measurements

### 3.5 Antithrombogenic property

To assess preliminary blood compatibility, platelet adhesion on the novel HBPI and HBPI-MPC film surfaces after contacting with PRP were evaluated by SEM observation. Figure 8 shows the representative SEM images of platelet adhesion of the novel HBPI and HBPI-MPC film surfaces with scanned areas of 63.9 μm × 44.8 μm. In the SEM images, the black circle-like substances are air pores which were formed in the films during thermal curing process, and the white points are the platelets. It can be seen from Fig. 8a that the number of platelets adhered to the surface of HBPI film is the highest, and most platelets in sight are deformed and stretched. The adhesion number of platelets on HBPI-5MPC and HBPI-10MPC films was reduced and platelets gradually separated with no aggregation. When the grafting amount of MPC reached 15%, the adhesion of platelets to the HBPI-15MPC film is significantly reduced. Moreover, few platelet cells adhered to the HBPI-20MPC film and they separated from each other with the morphology closer to the circle. Quantification of adhered platelets on the different samples is summarized in Table 2.

The recalcification times (RT) of HBPI-MPC films are intuitively displayed in Fig. 9 and summarized in Table 2. The determination principle of RT is the time of the recurrence of endogenous clotting process after re-adding $Ca^+$ to the plasma without $Ca^+$. As Fig. 9 shown, with the increase of MPC grafting amount, the RT of the films is constantly increasing from average 300 s of HBPI to average 551 s of HBPI-20MPC.

### 3.6 Antibacterial property

Figure 10a–e displays the SEM images of bacterial adherence of HBPI-MPC films. The antibacterial properties of materials were determined by counting the number of bacteria in the image. The bacterial counts (BC) of HBPI-MPC films were displayed in Fig. 10f and their statistics were in Table 2. With the increase of MPC grafting amount, the BC adhered to the surface of the films gradually decreased, indicating that the antibacterial properties of HBPI-MPC films were greatly improved.

## 4 Discussions

The purity of the triamine monomer TAPOB affects the properties of the synthesized hyperbranched polyimide. Thus, synthesise and purification of TAPOB are the primary conditions for the subsequent preparation of excellent anticoagulant hyperbranched polyimides. TAPOB was synthesized according to Chen's work [32]. The $^1$H NMR spectrum and infrared spectroscopy were used to accurately characterize the structure of TAPOB (Fig. 1). Each peak in the $^1$H NMR spectrum had a very good attribution, and no miscellaneous peaks appeared. And the characteristic absorption peaks of TAPOB just coincided with the measured infrared spectrum. The results indicated that the target triamine monomer TAPOB was successfully synthesized and very pure for later use.

The successful preparation of HBPI and HBPI-MPC films could be testified by FTIR and XPS. In FTIR spectrum, the disappearance of absorption band at 1660 $cm^{-1}$ indicated the complete imidization of HBPI, which was assigned to C=O stretching of amide. The absorption bands appeared at about 1773 $cm^{-1}$ (C=O asymmetrical stretching), 1721 $cm^{-1}$ (C=O symmetrical stretching), 1378 $cm^{-1}$ (C-N stretching) and 738 $cm^{-1}$ (C=O bending), which belonged to the characteristic peaks of imide. This proved the successful synthesis of HBPI. $N^+$ in the HBPI-MPC is in the form of a quaternary ammonium salt, while the quaternary ammonium salt has no characteristic absorption band. After the grafting reaction, the characteristic peak (P-O-(C)) of MPC appeared at 788 $cm^{-1}$ in the zoomed infrared curve (Fig. 2b, panel b), indicating that MPC had been grafted onto AM-HBPI via Michael addition reaction. In addition, the characteristic peak of amide (N-H) appeared at 3354 $cm^{-1}$ in Fig. 2a, panel b. This further proved that C=C on MPC reacted with terminal amino groups on AM-HBPI and the structure of amide was formed [34]. Furthermore, a more accurate testing method (XPS) was used to comfirm the successful grafting of MPC onto the HBPI. The XPS spectra (Fig. 3) clearly showed the emergence of P elements and variation of N element in the XPS curves of HBPI-MPC films. The reason why the N1s peak splited into two peaks in the XPS curve of HBPI film is that there were two forms of N elements in the HBPI structure. They were N elements in the imide ring and the terminal amino group respectively. After MPC was grafted onto AM-HBPI via Michael addition reaction, the terminal amino group of the

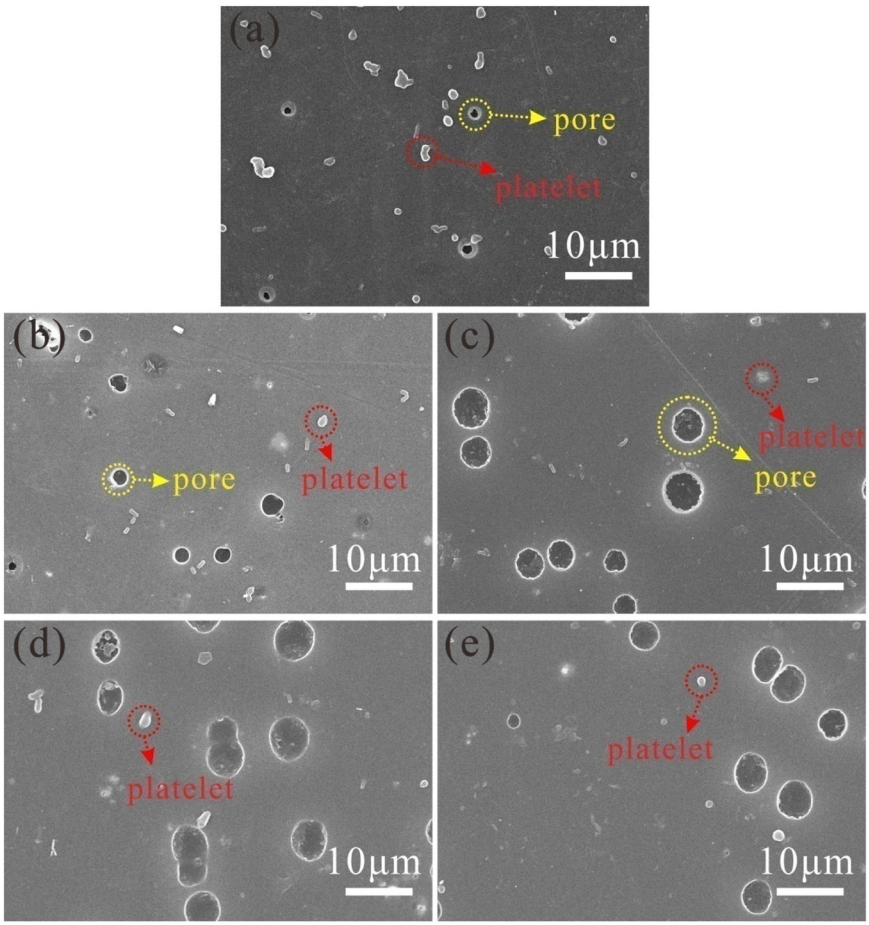


**Fig. 8** The SEM images of blood platelet adhesion of HBPI-MPC: **a** HBPI, **b** HBPI-5MPC, **c** HBPI-10MPC, **d** HBPI-15MPC, **e** HBPI-20MPC

**Table 2** Quantification of platelets, the recalcification times (RT) and the bacterial counts (BC) of HBPI-MPC films

| Samples | Number of adhered platelets (per $mm^2$) | RT(s) | BC (per $mm^2$) |
|---|---|---|---|
| HBPI | 11871 ± 254 | 300 ± 20 | 40402 ± 1005 |
| HBPI-5MPC | 8741 ± 179 | 325 ± 24 | 36783 ± 804 |
| HBPI-10MPC | 7342 ± 65 | 368 ± 25 | 32864 ± 703 |
| HBPI-15MPC | 3491 ± 43 | 505 ± 30 | 19698 ± 603 |
| HBPI-20MPC | 174 ± 21 | 551 ± 28 | 15678 ± 502 |

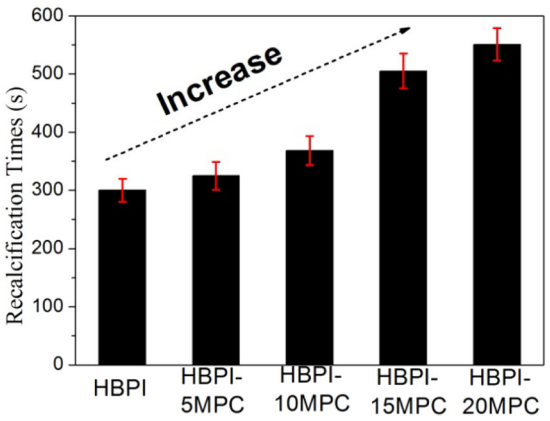


**Fig. 9** The recalcification times histogram of HBPI-MPC films

HBPI disappeared and the structure of amide was formed. The bond energy of the N element in the amide is basically the same as the N in the imide on the XPS spectrum. Therefore, only one peak (N1s) appeared in the XPS spectrum of HBPI-15MPC. These also showed that MPC was successfully grafted onto AM-HBPI. In summary, the results from the above FTIR and XPS characterization indicated that MPC molecules were successfully grafted onto HBPI molecules.

Polyimide is one of the best heat-resistant engineering plastics. Thermal performance is an important indicator for anticoagulant materials and directly affects the use of these anticoagulant materials. The TGA curves (Fig. 4) showed that the grafting of MPC had an effect on the thermal properties to some extent. The thermal stability of HBPI-MPC was reduced with the increase of MPC grafting amount. The change was mainly attributed to the thermal stability of MPC [35–37]. Because MPC contained a large number of C-O bonds, the thermal stability of MPC was lower than that of HBPI. Therefore, the more MPCs were

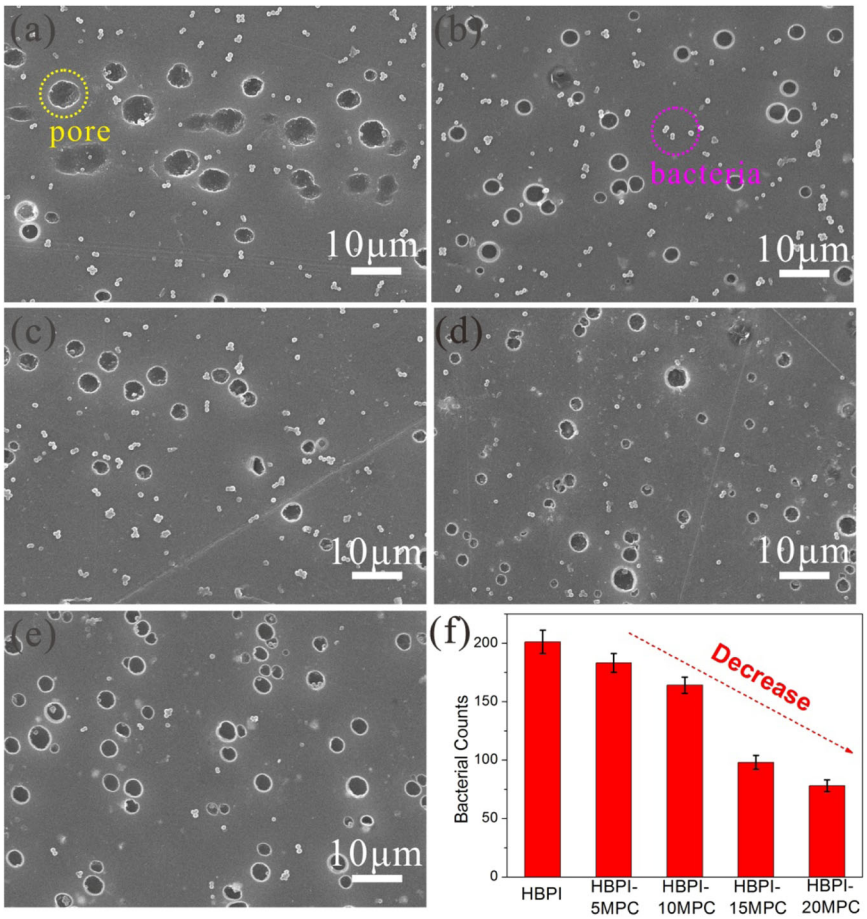


**Fig. 10** The SEM pictures of bacterial adherence of HBPI-MPC: **a** HBPI, **b** HBPI-5MPC, **c** HBPI-10MPC, **d** HBPI-15MPC, **e** HBPI-20MPC. **f** The bacterial counts (BC) of HBPI-MPC films

grafted, the more thermal stabilities of the HBPI-MPC films decreased. It was worth noting that the qualities of the matrixes (HBPI) of pure HBPI and HBPI-MPC films were set to equal in the experiment. MPC had undegradable chemical bonds at 800 °C in nitrogen, so the residual rates of HBPI-MPC films at 800 °C were higher than pure HBPI film in nitrogen. However, in general, all HBPI-MPC films still exhibited good thermal stability with no obvious weight loss before 350 °C. Their thermal stability will be a good guarantee during the use as anticoagulant materials.

The anticoagulation occurs at the interfaces between the blood and the anticoagulant materials. Therefore, the surface properties of them have a significant effect on the efficiency of anticoagulant. The results from WSCA showed that the neat HBPI film exhibited slightly hydrophilic property due to the hydrophilic imide rings and oxygen-containing linkages in the HBPI molecules. This result is similar to our previous work [20]. Moreover, the grafting of MPC greatly improved the hydrophilicities of the HBPI-MPC films. This phenomenon was attributed to the hydrophilic PC groups in MPC moleculars. Although the HBPI-MPC films exhibited increased surface roughness with the increase of MPC grafting amount, the Ra values of the HBPI-MPC films were still within nanometer scale. Therefore, it was reasonable to assume that they were relatively smooth for a large scale, for example, the scale of platelet (the diameter is about 3 μm) [38]. These changes of surface roughness would not result in platelet activation, aggregation and deformation when the films were in contact with blood. On the contrary, the number of exposed PC groups increased. Thereinto, PC groups possess excellent hydrophilic and biocompatibility. As a result, this graft modification facilitates its use in the field of biomedical materials.

The activation and adhesion of platelets on the surface of materials is an important cause of blood coagulation and thrombosis. When the blood contacts foreign matter, the adsorption first occurs for fibrin, albumin, globulin and other plasma proteins. Then pseudopodia deformation and adhesion occur for platelet. These deformations can cause thrombosis in plasma. Thus, the antiplatelet adhesion is the most intuitive and necessary index to evaluate the blood compatibility of biomaterials [33]. Figure 8 indicated that the platelets on the neat HBPI film may have been activated. It is proved that the pure HBPI film can not be used as anticoagulant material. The graft modification of HBPI is

necessary to enhance its biocompatibility. After surface graft modification, the adhesion number of platelets on the HBPI-MPC films gradually decreased, and the deformation and aggregation of platelets were also reduced with the increase of MPC grafting amount. The results demonstrated that the ability to resist platelet adhesion was associated with the grafting amount of MPC. After MPC molecules and PC groups were introduced into HBPI films, the structure on the surface of HBPI films was similar to the cell membrane. With the increase of MPC grafting amount, the MPC molecules on the surface of the film greatly increased. Thus, the platelet adhesion of the surfaces of HBPI-MPC films was reduced, rendering the blood compatibility of these films with a substantial improvement. The RT of HBPI-MPC films can also reflect their biocompatibility. The RT of the films constantly increased with the increase of MPC grafting amount (Fig. 9). As for anticoagulant materials, anticoagulant properties were improved with the increase of RT. Hence, the measured RT also demonstrate that the anticoagulant properties and biocompatibility of HBPI were greatly improved after the grafting of MPC.

Numerous studies showed that polymer materials with the structure of quaternary ammonium salt had excellent antibacterial properties and polymer antibacterial materials possessed many advantages such as long life, reusability and so on. In this experimental, staphylococcus aureus was selected as a strain. Staphylococcus aureus is an important human pathogen that causes many serious infections, especially at the wound. Moreover, staphylococcus aureus is ubiquitous in nature and can be found in air, water, dust, and human and animal waste. Therefore, there are many opportunities for food contamination. HBPI can be applied as wound dressings and food packaging. Hence, it is necessary to test the antibacterial activity of HBPI against staphylococcus aureus. It was seen from the result that the HBPI-MPC films had good antibacterial properties, owing to the existence of the structure of quaternary ammonium salt in MPC molecules. The increase of MPC grafting amount greatly improved the antibacterial properties of HBPI-MPC films. This performance will effectively reduce bacterial infection when the HBPI-MPC films are used as anticoagulant materials, such as blood bag, implanted material and so on.

## 5 Conclusions

In summary, AM-HBPI was successfully synthesized and completely imidized. The MPC molecules was then grafted onto the terminal amino groups of the AM-HBPI molecules using the Michael addition method, yielding MPC-modified hyperbranched polyimides (HBPI-MPC). The FTIR and XPS spectra proved the success of MPC grafting onto HBPI. The HBPI-MPC films exhibited slightly decreased thermal stabilities with 5% weight loss temperature in the range of 418–483 °C in nitrogen, compared with the pure HBPI film. But they still maintained good thermal stabilities, which guaranteed the stabity in use as anticoagulant materials. With the increase of MPC grafting amount, the static water contact angles of the HBPI-MPC films were gradually reduced and the surface roughness gradually increased. The increased surface roughness not only did not reduce the biocompatibility, but increased the anticoagulant performance of the HBPI-MPC films, because such planes on the surface of the HBPI-MPC films were still relatively smooth compared to the sizes of the platelets and the contact areas increased between anticoagulant MPC and platelets with the increase of MPC grafting amount. Moreover, in vitro platelet adhesion test indicated the number of platelets adhered to the surface of the HBPI-MPC films were reduced, and the morphologies of platelets changed from deformed ellipse to circle. The recalcification times (RT) increased from 300 s of HBPI to 551 s of HBPI-20MPC, indicating that the anticoagulant properties of HBPI-MPC films were greatly improved. Bacterial adhesion test also demonstrated the number of bacterial adhesion was significantly reduced for HBPI-MPC films, whose antibacterial properties were improved. Therefore, the HBPI-MPC films have the possibility of long-term use as biomedical instrument materials.

**Acknowledgements** The research was financially supported by the Natural Science Foundation of Hubei Province (2013CFB007), Hubei, China. Meanwhile, authors also acknowledge the Ministry of Education Key Laboratory for the Green Preparation and Application of Functional Materials for providing necessary facilities.

## Compliance with ethical standards

**Conflict of interest** The authors declare that they have no conflict of interest.

## References

1. Maitz MF, Zitzmann J, Hanke J, Renneberg C, Tsurkan MV, Sperling C, et al. Adaptive release of heparin from anticoagulant hydrogels triggered by different blood coagulation factors. Biomaterials. 2017;135:53–61.
2. Zhang Y, Yu J, Wang J, Hanne NJ, Zheng C, Qian C, et al. Drug delivery: thrombin-responsive transcutaneous patch for auto-anticoagulant regulation. Adv Mater. 2017; https://doi.org/10.1002/adma.201604043.
3. He M, Cui X, Jiang H, Huang X, Zhao W, Zhao C. Super-anticoagulant heparin-mimicking hydrogel thin film attached substrate surfaces to improve hemocompatibility. Macromol Biosci. 2017; https://doi.org/10.1002/mabi.201600281.
4. Amoako KA, Sundaram HS, Suhaib A, Jiang S, Cook KE. Multimodal, biomaterial-focused anticoagulation via superlow fouling zwitterionic functional groups coupled with anti-platelet nitric

oxide release. Adv Mater Interfaces. 2016; https://doi.org/10.1002/admi.201500646.
5. Fan W, Xu T, Zhao G, Meng S, Wan M, Bo C, et al. Mesoporous silica nanoparticles-encapsulated agarose and heparin as anticoagulant and resisting bacterial adhesion coating for biomedical silicone. Langmuir. 2017;33:5245–52.
6. Ma L, Cheng C, Nie C, He C, Deng J, Wang LR, et al. Anticoagulant sodium alginate sulfates and their mussel-inspired heparin-mimetic coatings. J Mater Chem B. 2016;4:3203–15.
7. Santerre JP, Woodhouse K, Laroche G, Labow RS. Understanding the biodegradation of polyurethanes: from classical implants to tissue engineering materials. Biomaterials. 2005;26:7457–70.
8. Losi P, Lombardi S, Briganti E, Soldani G. Luminal surface microgeometry affects platelet adhesion in small-diameter synthetic grafts. Biomaterials. 2004;25:4447–55.
9. Li Q, Liao GF, Tian J, Xu ZS. Preparation of novel fluorinated copolyimide/amine functionalized sepia eumelanin nanocomposites with enhanced mechanical, thermal, and UV-shielding properties. Macromol Mater Eng. 2018;303:1700407.
10. Seliktar D. Designing cell-compatible hydrogels for biomedical applications. Science. 2012;336:1124–8.
11. Kunzmann A, Andersson B, Thurnherr T, Krug H, Scheynius A, Fadeel B. Toxicology of engineered nanomaterials: focus on biocompatibility, biodistribution and biodegradation. BBA Gen Subj. 2011;1810:361–73.
12. Nakabayashi N, Iwasaki Y. Copolymers of 2-methacryloyloxyethyl phosphorylcholine (MPC) as biomaterials. Bio Med Mater Eng. 2004;14:345–54.
13. Hall B, Bird RR, Kojima M, Chapman D. Biomembranes as models for polymer surfaces: V. Thrombelastographic studies of polymeric lipids and polyesters. Biomaterials. 1989;10:219–24.
14. Kimura T, Nakaya T, Imoto M. Synthesis and polymerization of 2-(p-methacryloyloxybenzoyl)ethyl 2'-(phthalimido)ethyl hydrogen phosphate. Macromol Chem Phys. 1976;177:1973–9.
15. Ishihara K, Iwasaki Y. Biocompatible elastomers composed of segmented polyurethane and 2-methacryloyloxyethyl phosphorylcholine polymer. Polym Advan Technol. 2010;11:626–34.
16. Lee H, Dellatore SM, Miller WM, Messersmith PB. Mussel-inspired surface chemistry for multifunctional coatings. Science. 2007;318:426–30.
17. Ishihara K, Hanyuda H, Nakabayashi N. Synthesis of phospholipid polymers having a urethane bond in the side chain as coating material on segmented polyurethane and their platelet adhesion-resistant properties. Biomaterials. 1995;16:873–9.
18. Ishihara K, Tsuji T, Kurosaki T, Nakabayashi N. Hemocompatibility on graft copolymers composed of poly(2-methacryloyloxyethyl phosphorylcholine) side chain and poly(n-butyl methacrylate) backbone. J Biomed Mater Res A. 1994;28:225–32.
19. Li Q, Xiong H, Pang L, Zhang Y, Chen W, Xu Z, et al. Synthesis and characterization of thermally stable, hydrophobic hyperbranched polyimides derived from a novel triamine. High Perform Polym. 2015;27:426–38.
20. Zhang Y, Shen J, Li Q, Pang L, Zhang Q, Xu Z, et al. Synthesis and characterization of novel hyperbranched polyimides/attapulgite nanocomposites. Compos Part A Appl S. 2013;55:161–8.
21. Li Q, Wang Y, Zhang S, Pang L, Tong H, Li J, et al. Novel fluorinated random co-polyimide/amine-functionalized zeolite MEL50 hybrid films with enhanced thermal and low dielectric properties. J Mater Sci. 2017;52:1–14.
22. Li Q, Liao G, Zhang S, Pang L, Tong H, Zhao W, et al. Effect of adjustable molecular chain structure and pure silica zeolite nanoparticles on thermal, mechanical, dielectric, UV-shielding and hydrophobic properties of fluorinated copolyimide composites. Appl Surf Sci. 2017;427:437–50.
23. Starr P, Agrawal CM, Bailey S. Biocompatibility of common polyimides with human endothelial cells for a cardiovascular microsensor. J Biomed Mater Res A. 2016;104:406–12.
24. Mian A, Newaz G, Vendra L, Rahman N, Georgiev DG, Auner G, et al. Laser bonded microjoints between titanium and polyimide for applications in medical implants. J Mater Sci Mater Med. 2005;16:229–37.
25. Alfurhood JA, Bachler PR, Sumerlin BS. Hyperbranched polymers via RAFT self-condensing vinyl polymerization. Polym Chem. 2016;7:3361–9.
26. Alfurhood JA, Sun H, Bachler PR, Sumerlin BS. Hyperbranched poly(N-(2-hydroxypropyl) methacrylamide) via RAFT self-condensing vinyl polymerization. Polym Chem. 2016;7:2099–104.
27. Zhuang Y, Deng H, Su Y, He L, Wang R, Tong G, et al. Aptamer-functionalized and backbone redox-responsive hyperbranched polymer for targeted drug delivery in cancer therapy. Biomacromolecules. 2016;17:2050–62.
28. Giussi JM, Azzaroni O, Hensel-Bielowka S, Wojnarowska Z, Knapik J, Paluch M. Synthesis, characterization and dielectric relaxation study of hyperbranched polymers with different molecular architecture. Polymer. 2016;100:227–37.
29. Frangville C, Gallois M, Li Y, Nguyen HH, Lauthde VN, Talham DR, et al. Hyperbranched polymer mediated size-controlled synthesis of gadolinium phosphate nanoparticles: colloidal properties and particle size-dependence on MRI relaxivity. Nanoscale. 2016;8:4252–9.
30. Dai Y, Yu P, Zhang X, Zhuo R. Gold nanoparticles stabilized by amphiphilic hyperbranched polymers for catalytic reduction of 4-nitrophenol. J Catal. 2016;337:65–71.
31. Heckert B, Banerjee T, Sulthana S, Naz S, Alnasser R, Thompson D, et al. Design and synthesis of new sulfur-containing hyperbranched polymer and theranostic nanomaterials for bimodal imaging and treatment of cancer. ACS Macro Lett. 2017;6:235–40.
32. Chen H, Yin J. Synthesis and characterization of hyperbranched polyimides with good organosolubility and thermal properties based on a new triamine and conventional dianhydrides. J Polym Sci Pol Chem. 2002;40:3804–14.
33. Jiang H, Wang XB, Li CY, Li JS, Xu FJ, Mao C, et al. Improvement of hemocompatibility of polycaprolactone film surfaces with zwitterionic polymer brushes. Langmuir. 2011;27:11575–81.
34. Lu J, Feng Y, Gao B, Guo J. Grafting of a novel phosphorylcholine-containing vinyl monomer onto polycarbonateurethane surfaces by ultraviolet radiation grafting polymerization. Macromol Res. 2012;20:693–702.
35. Liao GF, Chen J, Zeng WG, Yu CH, Yi CF, Xu ZS. Facile preparation of uniform nanocomposite spheres with loading silver nanoparticles on polystyrene-methyl acrylic acid spheres for catalytic reduction of 4-nitrophenol. J Phys Chem C. 2016;120:25935–44.
36. Liao GF, Li G, Zhao WZ, Pang QH, Gao HY, Xu ZS. In-situ construction of novel silver nanoparticle decorated polymeric spheres as highly active and stable catalysts for reduction of methylene blue dye. Appl Catal A. 2018;549:102–11.
37. Xiao LJ, Deng M, Zeng WG, Zhang BX, Xu ZS, Yi CF, Liao GF. Novel robust superhydrophobic coating with self-cleaning properties in air and oil based on rare earth metal oxide. Ind Eng Chem Res. 2017;56:12354–61.
38. Chung TW, Liu DZ, Wang SY, Wang SS. Enhancement of the growth of human endothelial cells by surface roughness at nanometer scale. Biomaterials. 2003;24:4655–61.